POLITECNICO DI TORINO
Repository ISTITUZIONALE

Disproportionate collapse of a cable-stayed bridge

(Article begins on next page)

02 May 2024

Disproportionate collapse of a cable-stayed bridge

Author 1

- Marco Domaneschi, Assistant Professor
- Department of Structural, Geotechnical and Building Engineering, Politecnico di Torino, Turin, I
- http://orcid.org/0000-0002-6077-8338

Author 2

- Gian Paolo Cimellaro, Associate Professor
- Department of Structural, Geotechnical and Building Engineering, Politecnico di Torino, Turin, I
- https://orcid.org/0000-0001-6474-3493

Author 3

- Gianluca Scutiero
- Department of Structural, Geotechnical and Building Engineering, Politecnico di Torino, Turin, I

Full contact details of corresponding author.

Marco Domaneschi, Ph.D in Civil Eng.

Assistant Professor

Department of Structural, Geotechnical and Building Engineering

Politecnico di Torino

Corso Duca degli Abruzzi, 24

10129 Turin (TO) Italy

marco.domaneschi@polito.it, marco.domaneschi@gmail.com

Details:

http://www.diseg.polito.it/en/file/curriculum/(nominativo)/marco.domaneschi

Abstract

Disproportionate collapse of an existing cable-stayed bridge is investigated at the numerical level by employing a validated model from literature and the Applied Element Method. The earthquake input is used for the numerical simulations and applied at increasing intensity to assess the bridge response. The role of redundancy in the bridge structural scheme is proved as the strategic measure for avoiding disproportionate collapse and improving robustness. Therefore, an alternative configuration of the structural scheme has been assessed as possible countermeasure to improve the cable-stayed bridge response providing different loading paths against disproportionate collapse. With this aim, new redundancy indices that account the system reserve resources have been introduced.

Keywords chosen from ICE Publishing list
Bridge, Failure, Seismic Engineering

List of notation

σ normal stress

τ shear stress

f_u unidirectional limit stress

e_u unidirectional limit strain

ε longitudinal strain

γ shear strain

$(\sigma_y, \varepsilon_y)$ yielding point

$\{\varphi\}$ mode shape vector

S_0 displacement of the intact configuration

S_d displacement of the damaged configuration

ρ robustness index

R_u ultimate redundancy index

R_f functionality redundancy index

R_d damaged condition redundancy index

LF_1 load that origins the failure of the first structural member

LF_u load that is related to the achievement of the structural collapse

LF_f load that induces the overcoming of the functionality limit state in the intact structure

LF_d load connected to the collapse of the damaged structure (one member initially lost)

t_{FFM} time instant corresponding to the failure of the first structural member

t_{SC} time instant corresponding to the system collapse

t_{LF} time instant corresponding to the loss functionality

t_{UCDS} time instant corresponding to the ultimate capacity of the damaged system

$f(t)$ absolute value of the acceleration input

Introduction

Robustness of buildings and bridges is defined as the ability of the structure to withstand a given level of stress or demand (e.g. damage) without suffering degradation or loss of function. Besides, *redundancy* is another structural characteristic that is often required at the design level for the benefits it provides against unwanted behaviours. This last one is defined as the quality of having alternative paths in the structure by which the forces can be transferred, which allows the structure to remain stable following the failure of any single element (Cimellaro et al. 2010). Such characteristics, whose interconnection has also been recognised by Kanno and Ben-Haim (2011), are desirable in structural systems, being able to reduce vulnerability and therefore avoid disproportionate collapse. It occurs when an initial local failure that is produced by small triggering event leads to widespread failure of other structural components such that the structure collapses. It is also referred as progressive collapse (Starossek 2008, Starossek and Haberland 2010, Haberland et al. 2012).

In recent years several studies have been developed on structural collapses and much attention was paid for buildings, leaving the bridges' field still uncharted or partially investigated by few researchers (Wolff and Starossek 2009, Das et al 2016a). However, recent events of bridge collapses, namely in Genoa (Italy) on August 14th 2018 and in Kolkata (India) on September 4th 2018, have focused the public interest on the infrastructures' safety for their consequences in terms of fatalities and injuries, but also of economy and social losses.

The General Services Administration guideline (GSA 2003) and the Unified Facilities Criteria (UFC 2013) are the two most important guidelines that address progressive collapse in structures. However, they are focused on buildings and the progressive collapse of bridges is only briefly outlined in guidelines. E.g. according to the Posttensioning Institute (PTI 2012), the sudden loss of any one cable must not lead to the rupture of the entire structure.

Among the recent investigations, the structural behaviour of a long-span suspension bridge segmented by zipper-stoppers after the sudden rupture of some of its cables is studied in (Shoghijavan and Starossek 2018a). It has been found that increasing robustness of the structural system through segmentation is a possible approach to prevent progressive collapse in bridges due to cable failure.

The structural behaviour of long-span suspension bridges after the sudden rupture of a cable is studied in (Shoghijavan and Starossek 2018b, Shoghijavan and Starossek 2018c). The load carried by the failed cable must be redistributed to the other structural components and the cables adjacent to the failed cable receives most of the redistributed load becoming the critical member. Furthermore, cable failure produces large bending moments on the girder of the bridge. With the aim of studying these behaviour, a comprehensive analytical approach is proposed.

Moving to the cable-stayed-bridge class, Wang et al. (2017) investigate the collapse of a cable-stayed bridge due to strong seismic excitations, simulating the structural response through the explicit dynamic finite element method. They identified in the failure of piers and pylons the main reason for the collapse of cable-stayed bridge, rather than the failure of cables or main girder components. Their collapse mechanism under strong earthquake excitations is also investigated by Zong et al (2016). The results indicate that the ground motion action having the long predominant period cause the collapse of the bridge. The introduction of viscous dampers at the connections of the pylons and main girder can enhance the earthquake resistant collapse capacity of the bridge.

Das et al (2016b) introduced the Alternate Path Method to cable stayed bridges against their progressive collapse. The structural response is discussed for multiple types of cable loss cases to recognize the lack of robustness in the structure and to suggest more robust design options.

Wolff and Starossek (2009, 2010) investigated the disproportionate collapse of a cable-stayed bridge within a cable-loss scenario. The failure of three adjacent cables that stabilize the bridge girder in compression are responsible of the deck buckling as a result of high normal forces.

The importance of providing system redundancy was highlighted by the collapse of the Mississippi River Bridge in Minneapolis (Salem and Helmy 2017), Minnesota in 2007, in which the whole bridge, which has been classified as non-redundant by the National Transportation Safety Board (NTSB) (2008), catastrophically collapsed after the failure of a gusset plate connection.

With respect to the existing literature, the present paper analyses the response of a current cable-stayed bridge with respect to the issue of disproportionate collapse trough non-linear dynamic analysis and the use of the Applied Element Method (AEM). Furthermore, this research

proposes new redundancy indices that account the system reserve resources and quantitatively allow to evaluate alternative structural configurations.

A model of an existing bridge widely examined in literature (Li et al. 2014) through an international benchmark study on structural monitoring and control is used with the AEM and then validated. Solutions and interventions in order to avoid disproportionate collapse and increase bridge robustness and redundancy is analysed and discussed. The result is a new cable-configuration and deck strengthening.

The methodology is firstly discussed and the AEM is presented in the next sections. The bridge structure and the development of the numerical model with respect to the original benchmark problem are described. Finally, robustness and redundancy are examined in detail and the possible improvements with respect to seismic hazard are presented with the analysis results.

This study can provide valuable information that can facilitate decision making, enhance planning for disaster mitigation and recovering of critical infrastructures as the transportation network, reducing social and economic losses.

2. The methodology

Nonlinear dynamic analyses and the Applied Element Method are used to investigate the problem of disproportionate collapse in cable-stayed bridges. A methodology proposed in literature to quantify redundancy components has been extended to time history analyses.

A preliminary step consists of the calibration of an AEM model of an existing bridge with respect to a benchmark study available in the literature. Model Assurance Criterion has been used to validate the AEM model.

The numerical simulations are then developed for the original configuration of the bridge to analyse the problem of disproportionate collapse. The failure of more than two cables at mid-span is specifically considered. Subsequently a new cable-configuration to increase disaster resilience is studied.

The following sections are devoted to the presentation of the AEM and the model calibration for performing the subsequent numerical simulations on the bridge structure. The methodology proposed in literature to assess redundancy components is extended. Finally, the results of the numerical simulations are reported with concluding remarks.

2.1 The Applied Element Method

The proposed study investigates the progressive collapse of a real bridge through nonlinear dynamic analysis and an AEM based software (Applied Science International 2017). The AEM is an innovative modelling method that adopts the concept of discrete cracking (Domaneschi, 2012). Through two decades of continuous development, AEM was proven to be a method that can track the structural collapse behaviour passing through all stages of the application of loads: elastic stage, crack initiation and propagation in tension-weak materials, reinforcement yielding, element separation, element collision (contact), and collision with the ground and with adjacent structures. The possible analysis domain of the AEM in comparison to the Finite Element Method (FEM) is shown in Figure 1. Since its introduction in the early 1960s, the FEM has been the reference for the classic problems of structural mechanics. Therefore, it remains the most accurate for the elastic analysis of structures up to the solution of more complex problems (e.g. the nonlinear ones) (Zienkiewicz et al 2005). However, the onset of element separation remains difficult to automate within FEM and special routines have to be implemented to simulate such behaviour, in particular when three-dimensional dynamic analyses and solid elements are considered (Domaneschi 2012). Furthermore, modelling of debris collision is computationally demanding and time consuming in FEM. The AEM method, on the other hand, overcomes the difficulties of FEM in the simulation of the structural collapse and the debris distribution, while remaining reliable when used for common procedures, as the modal and the dynamic analyses (Applied Science International 2017).

Collapse History	FEM	AEM
Linear	Accurate	Reliable
Cracking – Yielding	Reliable	Reliable
Buckling	Reliable	Reliable
Elements Separation	Not Automated	Reliable
Debris Falling	Reliable	Reliable
Collision	Time Consuming	Reliable

Figure 1. Modelling of structure to AEM.

Within the AEM, the structure is modelled as an assembly of small elements that virtually subdivide the structure. Two elements are assumed to be connected by one normal and two orthogonal shear springs distributed on the elements adjacent faces, as shown in Figure 2.
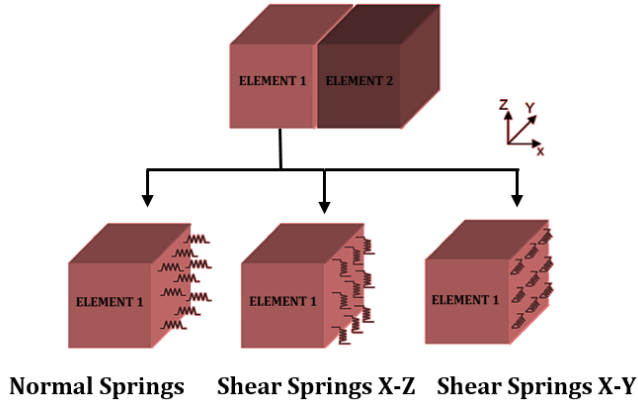

Figure 2. Spring interaction between elements in the AEM.

Each group of springs fully represents the stresses and deformations of the composite structure, e.g. reinforced concrete structures contain face-distributed springs triples for concrete material while the reinforcement steel bars are modelled explicitly. If there is a rebar running through the interface of two cuboids, a spring representing the rebar is assigned to the interface.

These springs allow also to implement the failure criteria properties associated to the structural component, as discussed in the next subsection. The springs' generation is automatically performed in the AEM software Extreme Loading for Structure (Applied Science International 2017).

2.2 Element separation criteria and failure criteria

The average normal strain is calculated by averaging the absolute values of strains on each face of the elements. When the average strain between these two adjacent faces reaches a threshold called the separation strain – which is specified in the material property – the springs between these two faces are removed and it is assumed that these elements behave as two separate rigid bodies for the remaining analysis. Separation strain represents the limit at which adjacent elements are totally separated at the connecting face as shown in Figure 3. Therefore,

the refinement level of the discretisation is a significant parameter to be calibrated to accurate reproduce the structural collapse.
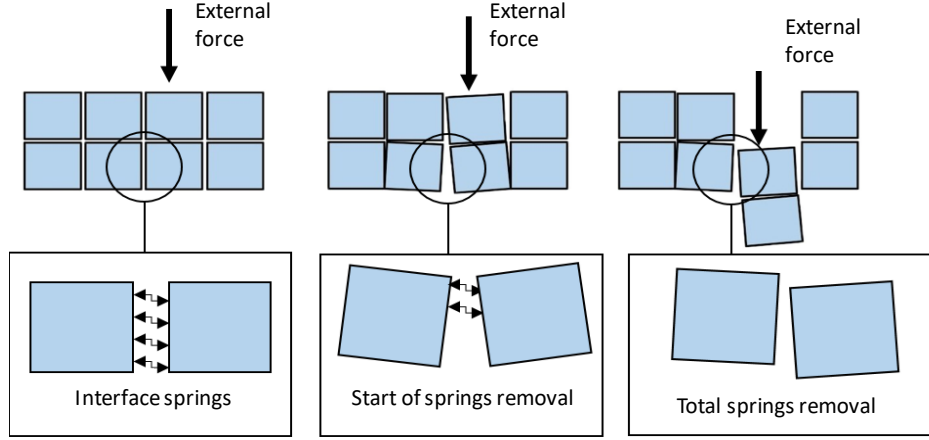

Figure 3. Separation phases.

According to Meguro et al. (2000), the springs that simulate the steel reinforcement bars in a composite material are removed if the internal stresses reach the failure criteria defined in Eq. (1).

$$f_u = \sqrt{\sigma^2 + \tau_1^2 + \tau_2^2}$$
<div align="right">1.</div>

where σ, τ_1, τ_2 are the normal and shear stresses respectively and f_u is the tensile limit stress of the reinforcement bar. Alternatively, the spring is removed if the internal strains reach the unidirectional limit strain e_u defined in Eq. (2).

$$e_u = \sqrt{\varepsilon^2 + \gamma_1^2 + \gamma_2^2}$$
<div align="right">2.</div>

where ε, γ_1, γ_2 represent the longitudinal and shear strains respectively. One of the features of AEM is the *automatic element contact detection*. Elements may collide each other, separate and collide again. There are three types of collisions: (i) element corner-to-element face, (ii) element edge-to-element edge and (iii) element corner-to-ground (Applied Science International 2017).

2.3 AEM solution for cable modelling

Using the AEM the cables of the bridge can be included as *link members*. The link member is a special spring that has the ability to connect two separate solid elements with any angle of inclination, carrying axial stresses only.

In order to reproduce the cables performance, a *tension-only bilinear material* is assigned. As shown in Figure 4, the bilinear constitutive law of the material shows a linear trend with elasticity modulus E up to the yield point $(\sigma_y, \varepsilon_y)$ without any plastic deformations. After yield, plastic deformations take place and the stress-strain post-yield relation behaves linearly up to failure. After failure, the strength drops to zero but springs remain till they reach separation strain where the elements are fully separated from each other and springs no longer exist. A stress-softening parameter is used after failure. Tension-only bilinear material is a special case of the bi-linear material where the elements can carry only tensile stresses.
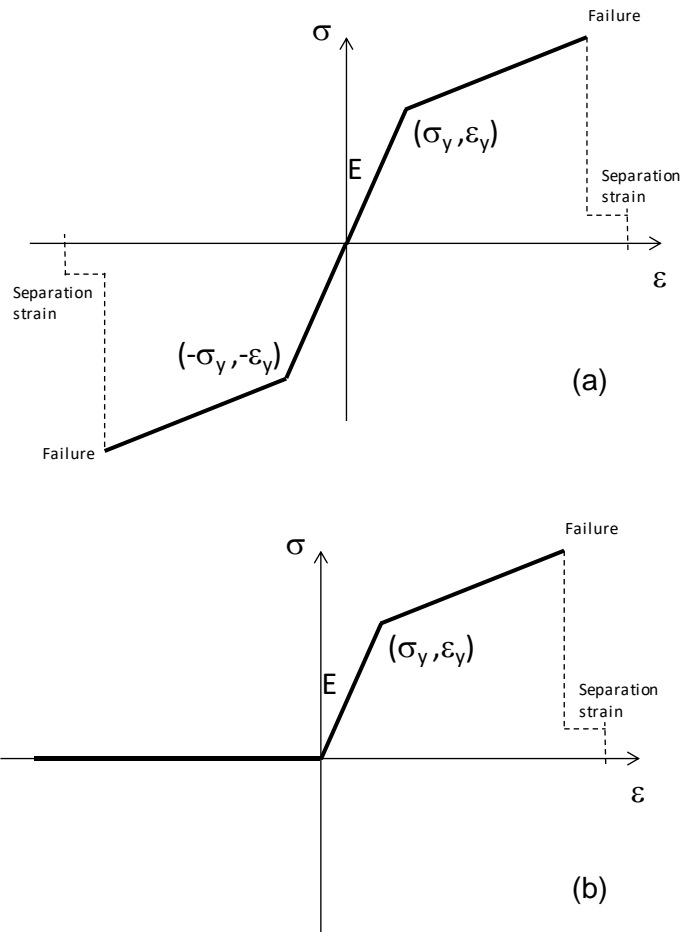

Figure 4. Stress-strain constitutive law of a bilinear material (a). Tension-only case (b).

3. The AEM model

3.1 The bridge structure

The analysed bridge is the Yong-he bridge (Tianjin, built 1981-1987, designed by the Tianjin Municipal Engineering Survey and Design Institute). It is one of the first cable-stayed bridges constructed in mainland China (Figure 5) and was opened to traffic in December 1987. It has two main spans of 260 m and two side spans of 25.15 + 99.85 m each. The whole bridge is 510 m long and 14.5 wide. The main girder was assembled from 74 precast concrete girder segments that are formed continuously by cast-in-place joints that connect the girder ends and form transversely reinforced diaphragms. The prestressed girder of the side span was built on site using formwork supported by temporary falsework. The concrete bridge towers, connected by two transverse beams, are 60.5 m tall and was constructed using sliding formwork technology.

There are a total of 88 pairs of cables containing steel wires of 5 mm in diameter. Each cable can contain between 69 and 199 steel wires (5mm in diameter). The design cable tension forces under dead load range from 559.4 to 1706.8 kN (the stress is approximately 450MPa), and the design stress in the cables due to live load is 160MPa.

The Yong-he bridge is the subject of an international benchmark proposed by the Centre of Structural Monitoring and Control at the Harbin Institute of Technology. The benchmark structure with the details on the geometry, the design tables with the cross sections of the towers and the main girder, the foundations, and the material properties are reported in (Li et al. 2014).
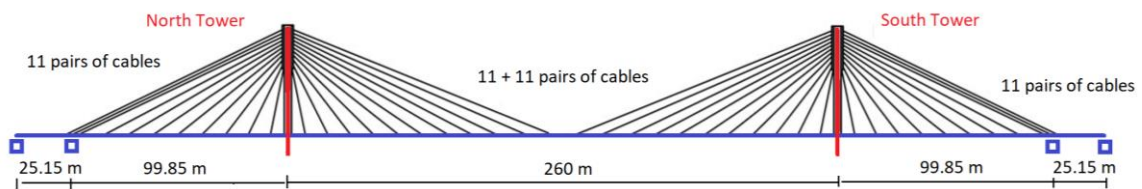

Figure 5. Yong-he bridge geometry.

3.2 The bridge model

The complete description of the finite element model of the bridge in the Ansys code with the model updating procedure is presented in detail in the benchmark statement. The finite element

model of the bridge has been validated through on the basis of the field monitoring data from the full-scale bridge (Li et al. 2014). It was developed on the basis of the engineering drawings and originally implemented using the ANSYS software. Three-dimensional beam elements were used to model the bridge towers and the main girder. The cables were modelled using linear elastic link elements (uniaxial tension-only elements). The main girder ass restrained by the stay-cables, the towers and the piers, while these last ones were fixed to the ground. The longitudinal restriction effect of the rubber supports was simulated using linear elastic spring elements.

In this study the original benchmark model was consistently replicated using the AEM. The material parameters that have been used in the original benchmark have been implemented in the AEM model.

A preliminary linear static analysis was carried out on the original configuration of the bridge under the dead weight of the structural elements. The displacement field thus obtained was subsequently used to update the position of the nodes in the global model of the bridge: the coordinates of the nodes in the undeformed configuration were modified according to the displacements resulting from the static analysis under self-weight only. The bridge model obtained in this way matches the geometry envisaged in the original benchmark model, while taking into account the state of pre-stress induced by the mass density (Domaneschi et al. 2016).

The AEM model has been finally validated through a comparison in terms of natural frequencies and mode shapes. The criterion used to verify the correlation between modes is the Modal Assurance Criterion (MAC). According to Pastor et al. (2012), the MAC is a statistical indicator that is most sensitive to large differences and relatively insensitive to small differences in the mode shapes. The MAC is calculated as the normalized scalar product of the two sets of vectors $\{\varphi_A\}$ and $\{\varphi_B\}$. The resulting scalars are arranged into the MAC matrix.
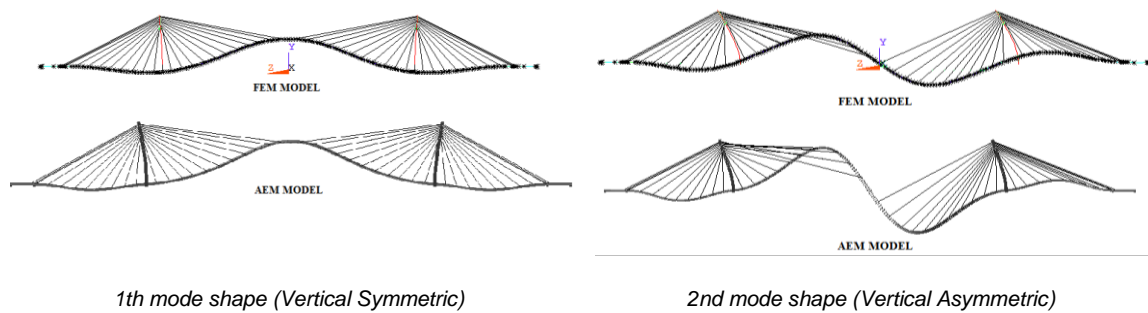
$$MAC(r,q) = \frac{\left| \{\varphi_A\}_r^T \{\varphi_x\}_q \right|^2}{\left(\{\varphi_A\}_r^T \{\varphi_A\}_r \right) \left(\{\varphi_x\}_q^T \{\varphi_x\}_q \right)} \qquad 3.$$

The MAC takes value between 0 (representing no consistent correspondence) and 1 (representing a consistent correspondence). Values larger than 0.9 indicate consistent

correspondence whereas small values indicate poor similarity between two shapes. Seven shape modes are taken into account as shown in Table 1. Figure 6 reports the comparison of the seven mode shapes detailed in Table 1 between the FEM and the replicated AEM.

Table 1. Mode shapes. Vertical Symmetric = V.S., Vertical Asymmetric = V.A., Transverse Asymmetric = T.A.

Mode Nr.	FEM Frequency [Hz]	AEM Frequency [Hz]	Shape -	∆Frequency [%]	MAC -
1	0.417	0.416	V.S.	0.24	0.991
2	0.593	0.643	V.A.	-7.78	0.978
3	0.877	1.012	V.S.	13.34	0.945
4	1.044	1.297	V.A.	19.51	0.946
5	1.089	1.349	V.S.	19.27	0.930
6	1.213	1.515	V.A.	19.93	0.889
7	0.311	0.280	T.A.	11.07	0.928

1th mode shape (Vertical Symmetric)   2nd mode shape (Vertical Asymmetric)

3rd mode shape (Vertical Symmetric)

4th mode shape (Vertical Asymmetric)

5th mode shape (Vertical Symmetric)

6th mode shape (Vertical Asymmetric)

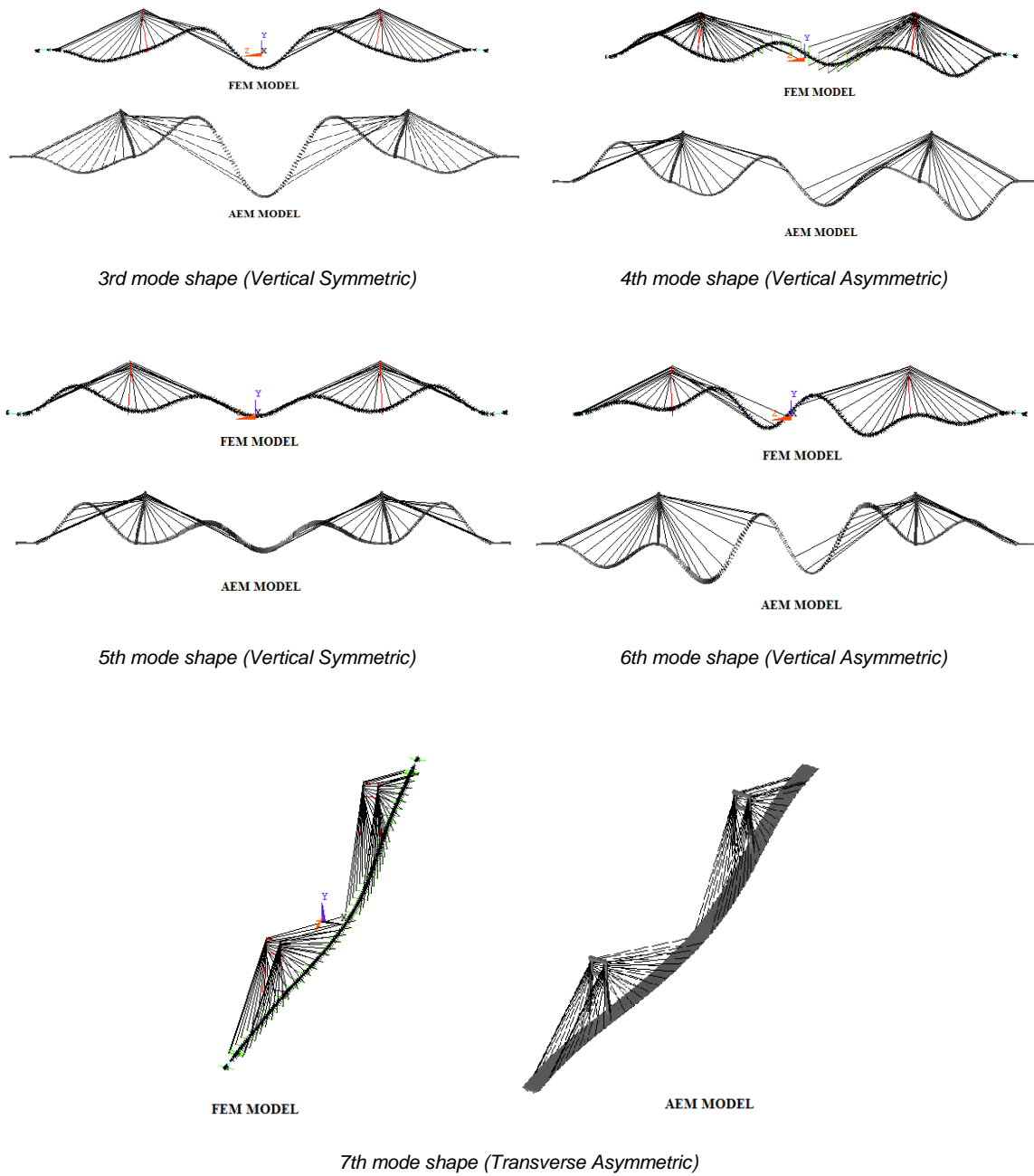*7th mode shape (Transverse Asymmetric)*

Figure 6. Comparison between FEM and AEM models in terms of mode shapes.

A static comparison in terms of vertical displacements response along the symmetry axis of the bridge due to dead load was also performed. The displacement value at mid-span is shown in Table 2, while a graphic comparison in terms of structural deformed shape is presented in Figure 7.

Table 2. Vertical displacements at the mid-span of the FEM and the AEM models.

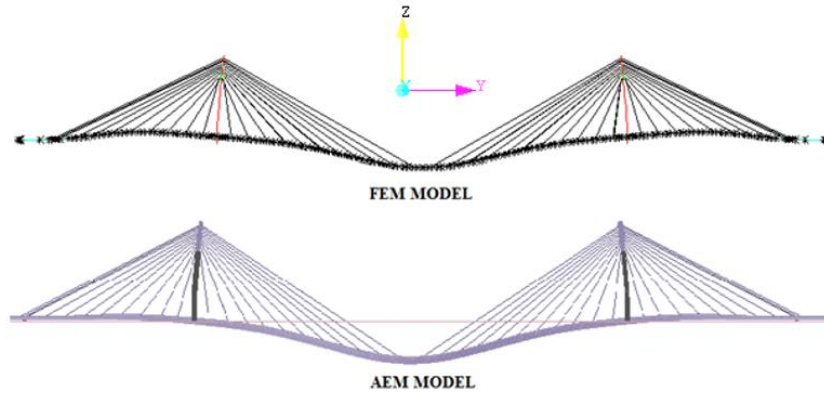| Model	Vertical displacement	Δ
	[m]	[%]
FEM	0.178	
AEM	0.163	9

Figure 7. Deformed shape: FEM model and AEM.

4. Robustness and redundancy issues

Several competing approaches for the deterministic evaluation of structural robustness and redundancy have been discussed by Anitori et al. (2013). Biondini and Restelli (2008a, 2008b) evaluated robustness using an index that relates the global displacements of a structure composed of parallel members in different configurations:

$$\rho = \frac{S_0}{S_d}$$ 4.

where S_0 is the displacement of the intact configuration of the system and S_d is the displacement of the damaged configuration. This robustness index ρ decreases from 1 and approaches to 0 as damage spreads within the system. The significance of ρ is that it is a measure of the system susceptibility to damage spreading through the structural elements.
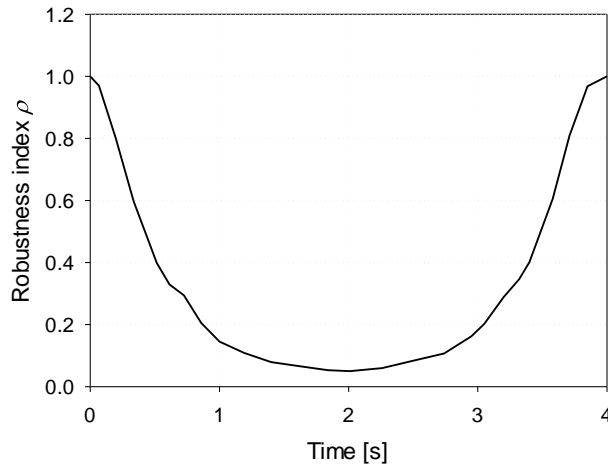
Figure 8. Robustness curve.

A no-damage configuration of the bridge within the linear elastic field subjected to dynamic action, was initially tested and this resulted in a robustness index variation as shown in Figure 8. On the horizontal and vertical axes respectively, the time and the robustness index ρ are presented. The model is subject to a low-intensity impulsive perturbation. After 2s the maximum effect for the response of the structure is reached and in the following 2s the original configuration is recovered as the model in this case is linear elastic. In this case the value s_0 represents the displacement of the bridge configuration at rest (gravitational loads), while s_d is the displacement of the bridge configuration when both dynamic loads (impulsive perturbation) and gravitational loads are considered. Indeed, using Eq. 4, the increasing displacements resulting from perturbation cause the value of the robustness index to decrease. As the external dynamic perturbation decreases, the structure tends to return to the initial configuration and the robustness index increases to unity. If the structure is outside the linear elastic range, damage can be verified: the ascending part of robustness curve would be reduced or totally absent due to the presence irreversible deformation.

Structural redundancy is defined by Ghosn and Moses (1998) and Liu et al. (2000) as the capability of the system to continue to carry load after the failure of one main member. They proposed three different indices to assess redundancy components. Two indices are related to the overloading of the originally intact configuration of the structure and are defined as the ability to withstand collapse and/or to avoid losses in the structural functionality. The third index is

computed for a damaged configuration of the structure and allows the assessment of the system capability to carry extra loads after the damage occurrence in one main structural member.
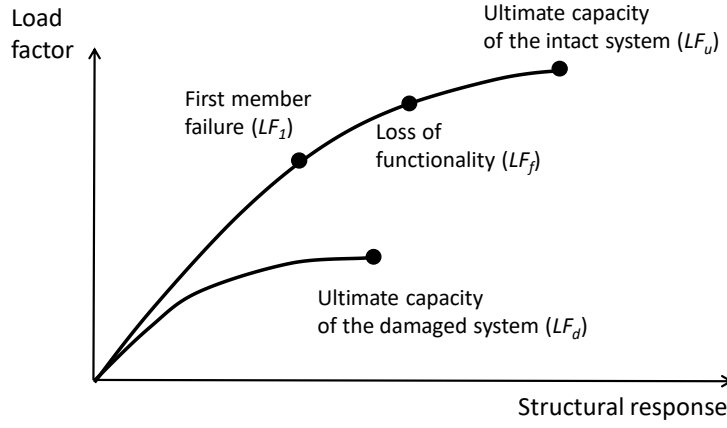

Figure 9. Load measures needed to calculate redundancy indices.

The redundancy indices are defined in terms of the system reserve ratios (Liu et al. 2000) such as R_u, R_f, R_d for the ultimate, functionality and damaged condition limit states, respectively (Figure 9). They are computed with respect to the load that origins the failure of the first structural member and are given by following equations:

$$R_u = \frac{LF_u}{LF_1}$$ 5.

$$R_f = \frac{LF_f}{LF_1}$$ 6.

$$R_d = \frac{LF_d}{LF_1}$$ 7.

Where LF_1 is the load that causes the failure of the first structural member, LF_u the load that is related to the achievement of the structural collapse, LF_f the load that results in loss of functionality in the intact structure, LF_d the load causes collapse of the damaged structure (with one main member initially lost). In other words, R_u, R_f, R_d indices measure the system's

capacity to withstand first member failure and can be used to evaluate alternative design solutions.

In this paper, an algorithm to extend the methodology proposed by Liu et al. (2000) using history analysis is presented. The original methodology was related to *pushover* analyses, therefore the (nonlinear) static domain was considered only. If nonlinear dynamic analyses are considered, the load factor method cannot be used and a different approach has to be developed.
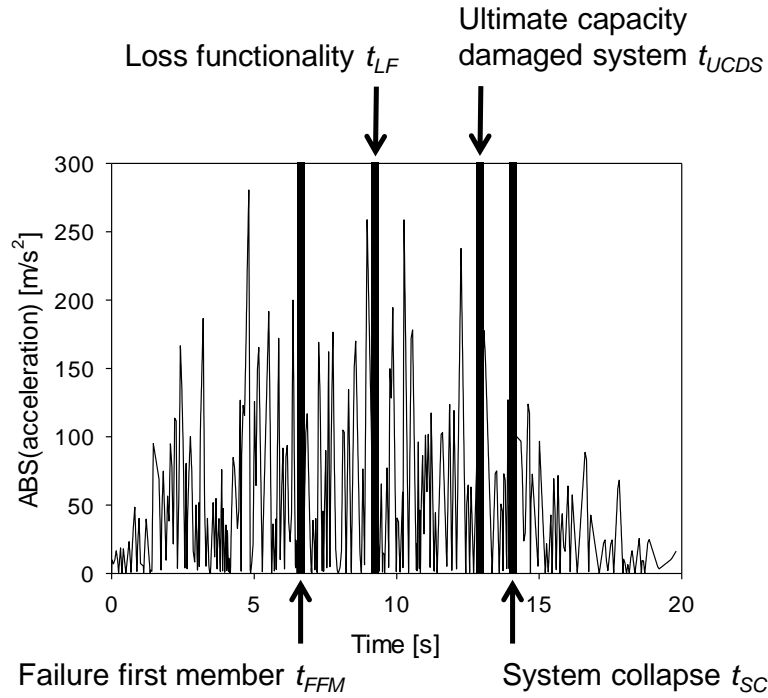

Figure 10. Absolute value of the acceleration input.

In the first step of the proposed procedure, the acceleration input is converted to positive values only. In the second step, the acceleration input is integrated between 0 and the time instant corresponding to the failure of the first structural member (t_{FFM}) to compute an equivalent value for LF_1 load level in the case of time history analysis. This value is critical for the computation of the redundancy indices because they account the system's capacity to withstand first member failure with respect to ultimate, functionality and damaged condition limit states.

Integrating between the time corresponding to the failure of the first member and the system collapse time (t_{SC}), an equivalent value of LF_d load is obtained. Following the same procedure, LF_f and LF_u loads can be computed. Theoretically, the integral of the acceleration input

related to structural collapse or functionality losses will be higher than the integral that causes the first component failure. Figure 10 summarizes the adopted conditions for the computation of the proposed indices.

$$LF_1 = \int_0^{t_{fFFM}} f(t)dt \qquad\qquad 8.$$

$$LF_u = \int_0^{t_{SC}} f(t)dt \qquad\qquad 9.$$

$$LF_f = \int_0^{t_{LF}} f(t)dt \qquad\qquad 10.$$

$$LF_d = \int_0^{t_{UCDS}} f(t)dt \qquad\qquad 11.$$

Where $f(t)$ is the absolute value of the acceleration input. Therefore, the numerical procedure consists in the integration of linear functions that are defined through the discretization of the time history in Figure 10. Indeed, the transition between each sample of the time history is linearly approximated. It means that straightforward approaches, as the trapezoidal rule, can be also employed for the numerical integration of $f(t)$.

5. Seismic response simulation of the Yong-he bridge

5.1 Original configuration of the structure

The effect of cable failure is investigated by nonlinear dynamic analyses in the time domain taking into account large deformations. Direct time integration is used to solve the equations of motion. The input accelerogram computed by Haifan (1983) to analyse the influence of phase-difference effect on the earthquake response of the Yong-he bridge was used for the numerical simulation of this study (Figure 11a). The results of the corresponding AEM analyses highlight the disproportionate collapse shown in Figure 11b.
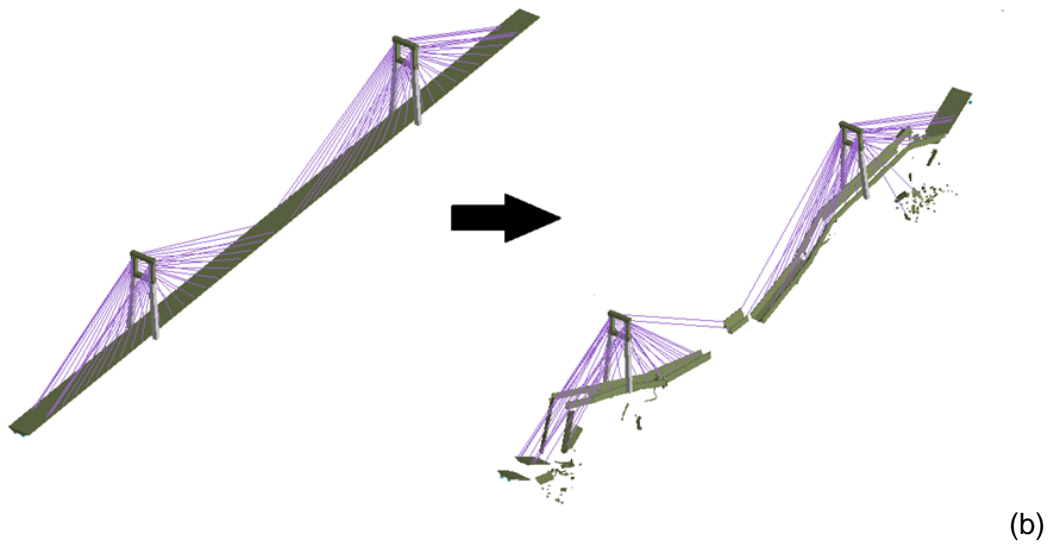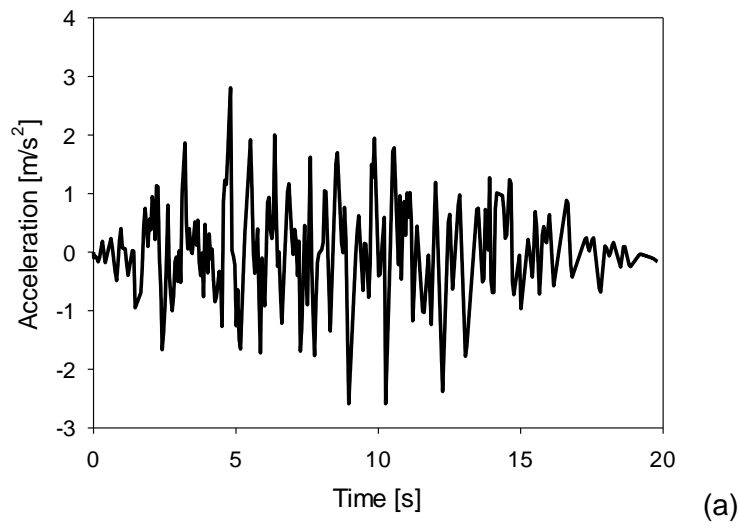
Figure 11. (a) Input accelerogram computed by Haifan (1983). (b) Disproportionate collapse from AEM simulations.

In order to analyse the structural problem and identify the collapse mechanism, cable stresses are evaluated. In particular the cables highlighted in Figure 12 were considered. The maximum values of cable stresses are shown in Table 3.
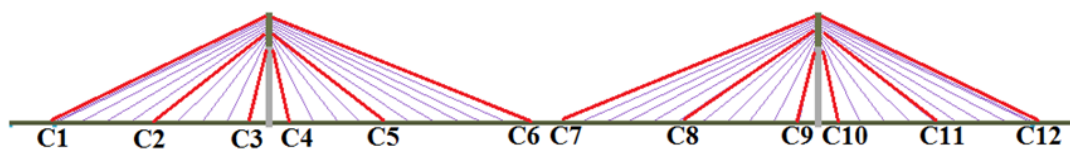

Figure 12. Analysed cables.

Table 3. Maximum axial stresses in the cables.

Cable	σ_{MAX}	$time(\sigma_{MAX})$
	MPA	s
C1	365	6.2
C2	367	11.3
C3	386	13.1
C4	417	13
C5	468	12
C6	468	6.2
C7	468	7.5
C8	468	8
C9	444	8.8
C10	363	5.1
C11	396	16
C12	365	6

Figure 13 shows the stress time history in cables C6 and C7 from the AEM simulation where the time of the failures can be observed. Cable C6 fails at about 7 seconds when the input acceleration highlights an intensity peak. The weakening of the support system due to the failure of cable 6 leads to the failure of cable 7 after about 1 second. Both C6 and C7 are the longest cables of the suspension system, supporting the mid-span of the bridge. As reported by Li et al. (2014), the design ultimate stress for the cables is about 460 MPa, consistently with the simulations.
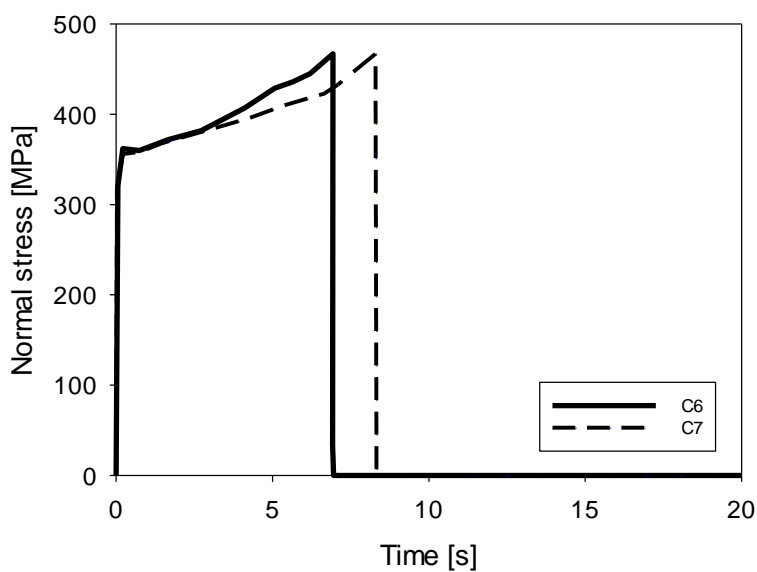

Figure 13. Normal stress in cable C6 and C7.

Failure of cables C6 and C7 cause the overloading of the structural members and consequently further ruptures of adjacent cables. The cables losses lead to a reduction of the capacity of the supporting system and increase the risk of the global failure of the structure. As a result, the bridge collapse due to progressive shocks of the ground motion cannot be avoided. Wolff and Starossek (2010) report that this phenomenon occurs when the distance between the first failed cable and the adjacent cables is about 10 metres.

In Figure 14, the robustness variation with respect to time is reported. After the failure of cable C6, the robustness decreases until the collapse of the entire bridge (disproportionate collapse). The redundancy indices take the values: $R_u = 1.71$, $R_f = 1.09$, $R_d = 1.21$.
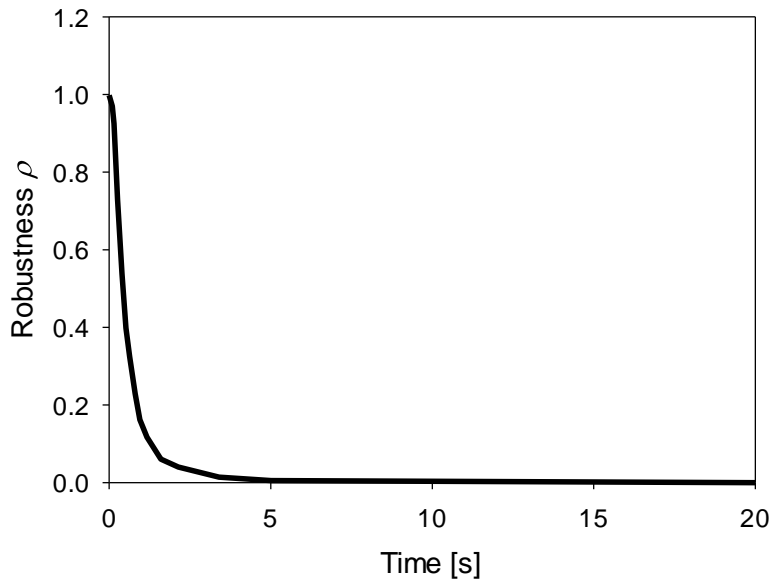

Figure 14. Variation of robustness with respect to time.

The analysis of the disproportionate collapse of the bridge presented here, together with the review of the existing literature, has led to some considerations of an alternative cables configuration that will be described in detail in the next section.

5.2 Modified configuration of the structure

A new configuration for the cables in the central span of the bridge is proposed to improve the bridge response. As shown in Figure 15a, the distance between the cable-deck connection is

reduced while the cross-sections have been retained. For cables adjacent to the mid-span (e.g. C6 and C7) the spacing is fixed at 8 m, while the cables adjacent to the towers (e.g. C4 and C9) are at 10 m. This configuration results in a reduction of the stress in the cables, and cables C6 and C7 in particular at the mid-span that have been identified as the responsible of the disproportionate collapse.

The new configuration is also in agreement with Shoghijavan and Starossek (2018b, 2018c) that suggest to redistribute the load carried by the failed cable to other structural components (as adjacent cables).

The analyses of the new configuration of the deck show localized damage at the deck mid-span, as shown in Figure 15b, and disproportionate collapse of the bridge is avoided. The failure of the main girder is due to high tensile stresses.
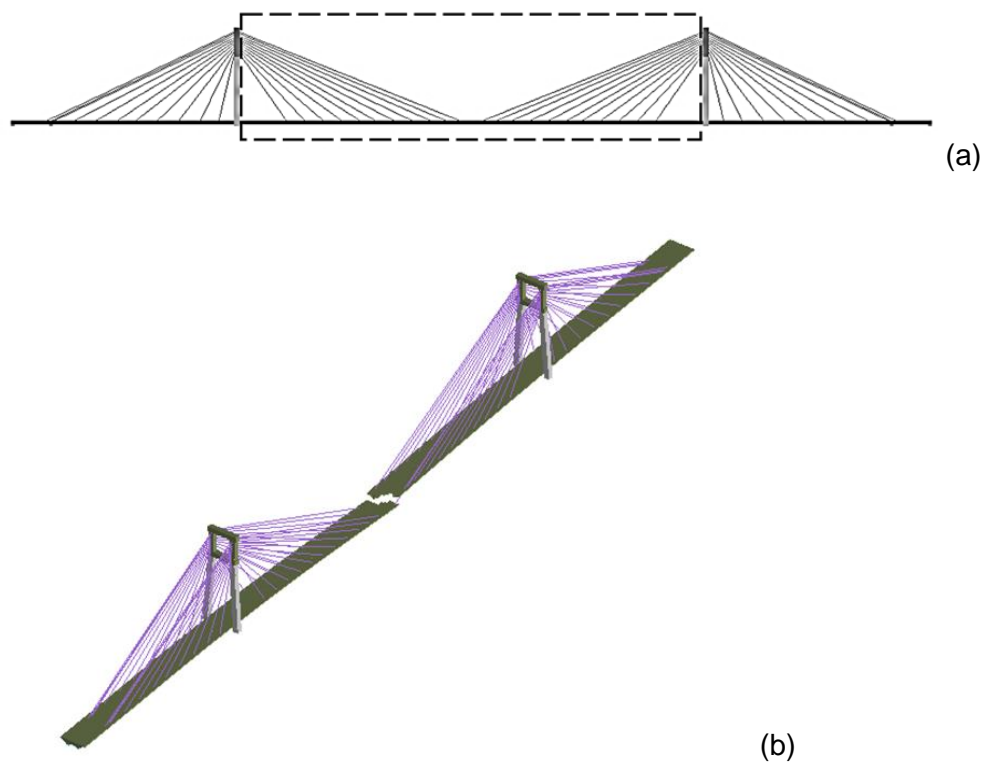

(a)

(b)

Figure 15. (a) New cable configuration and (b) the corresponding AEM model of the bridge.

The normal stresses in the longest cables of the new configuration are shown in Figure 16. They can be compared to those of cables C6 and C7 in Figure 13. A perturbation in the response occurs at the deck mid-span failure (time range 10-15 s) .
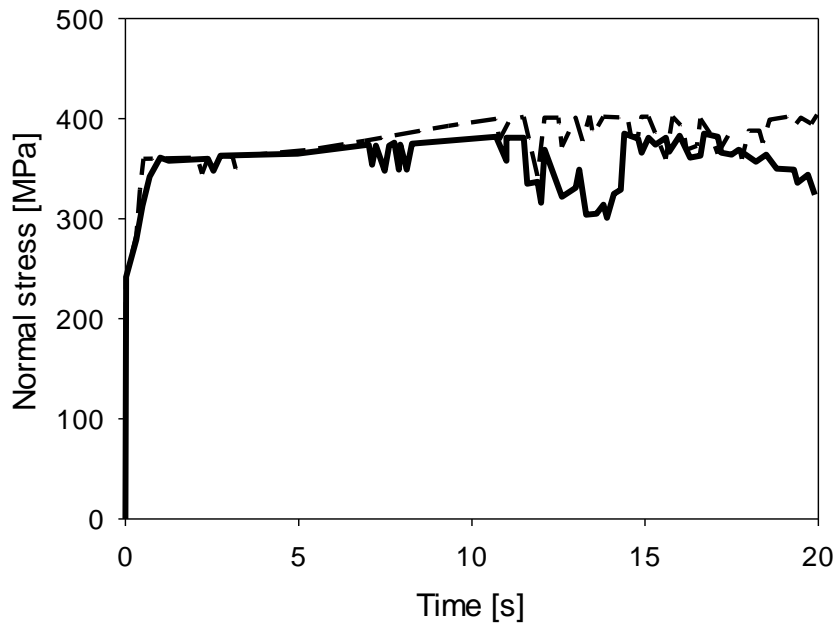
Figure 16. Axial stresses in the longest cables for the new configuration of the bridge.

The lateral strength of the reinforced concrete deck is abruptly reduced after reaching its ultimate deformation due to rupture of the steel reinforcing bars or concrete crushing. In Table 4 the maximum values of the normal stress in the cables are shown. They remain lower (even if close) than their ultimate limits.

Table 4. Maximum axial stresses in the stay-cables for the new configuration of the bridge.

Cable	σ_{MAX}	$time(\sigma_{MAX})$
	MPa	sec
C1	380	C1
C2	379	C2
C3	372	C3
C4	375	C4
C5	379	C5
C6	381	C6
C7	404	C7
C8	370	C8
C9	373	C9
C10	375	C10
C11	373	C11
C12	371	C12

The deck displacements from the numerical simulations are extracted and the robustness index is calculated for each time step as shown in Figure 17. The redundancy indices values results the following: $R_u = 4.34$, $R_f = 2.71$, $R_d = 3.37$.

Comparing the values of the redundancy indices of the original bridge configuration, a remarkable improvement in terms of redundancy is highlighted. This results from the evaluation of the robustness index leading to performance over the previous configuration of the bridge (Figures 17 and 14).
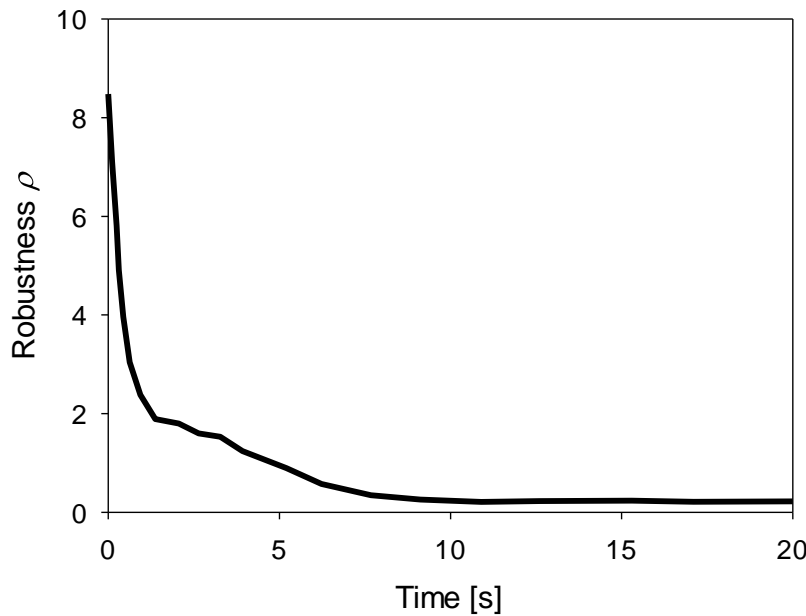

Figure 17. Robustness variation with respect to time for the new configuration of the bridge.

6. General remarks

Numerical analyses have the benefit of being able to effectively control the changes introduced in the modified structural configuration maintaining all other conditions unchanged. This allows a consistent comparison in terms of structural response between the original configuration and the alternative.

The problem of double-cable-losses for the cable stayed-bridge is considered with respect to the disproportionate collapse and the way to improve redundancy is investigated through nonlinear time history analyses. It is worth noting how such local failure condition improves the

requirements of the existing PTI Recommendations. Indeed, they require that a cable-stayed bridge shall be capable of withstanding the loss of any one cable (PTI 2012). Therefore, the proposed alternative configuration of the cable-stayed bridge is able to give additional benefits with respect to the minimum expected requirements.

With respect to the existing literature, new redundancy indices are proposed for time history analyses. They introduce a new information, allowing a quantitative measure of redundancy. In particular, the proposed alternative bridge configuration (section 5.2), with respect to the original one (section 5.1), shows how the reduction of the geometrical distance between the cables-deck connection can uniformly improve all redundancy indices of about 250%. It means that the system is capable to withstand local cables failure with uniform reserve ratios, with respect to ultimate, functionality and damaged condition limit states.

The improvements highlighted by the redundancy indices between the alternative and the original bridge configurations are reflected also in the robustness index ρ, in agreement with the recognised relation between redundancy and robustness (Kanno and Ben-Haim 2011). Indeed, ρ parameter results essentially improved in the first half of the analysis (range 0-10 s in Figure 17). However, the deck mid-span failure affects the second part of the diagram.

7. Conclusion

The problem of disproportionate collapse of an existing cable-stayed bridge is investigated through nonlinear dynamic analysis and the Applied Element Method. An algorithm is presented to extend a methodology proposed in literature using time history analysis to compute redundancy indices in terms of the system reserve ratios.

The analyses of the cable-stayed bridge model show that the bridge cannot sustain the failure of more than two cables at mid-span without resulting in a disproportionate collapse. In addition, disproportionate collapse can be avoided through a new cables-configuration. This is closely connected with improvements in robustness and redundancy. However, the new configuration is not enough to guarantee the functionality of cable-stayed bridge after a strong motion event, because the stresses in the bridge deck compromise the structural stability. Therefore, additional strengthening would be necessary in the main girder to overcome this issue and avoiding functionality losses. The methodology can support decision-makers to explore the

performance of bridge structures in seismic affected area, to plan strategies and resilience improvements to minimize both losses and recovery time.

Acknowledgements

References

Anitori G, Casas JR and Ghosn M (2013) Redundancy and Robustness in the Design and Evaluation of Bridges: European and North American Perspectives. Journal of Bridge Engineering 18(12):1241-1251.

Applied Science International, LLC (ASI) (2017) Extreme loading for structures Theoretical Manual - Extreme loading for structures 5.0. Applied Science International.

Biondini F and Restelli S (2008a) Damage propagation and structural robustness. Life-Cycle Civil Engineering – Biondini and Frangopol (eds), Taylor and Francis Group, London, ISBN 978-0-415-46857-2.

Biondini F and Restelli S (2008b) Measure of structural robustness under damage propagation. Bridge Maintenance, Safety, Management, Health Monitoring and Informatics - Proceedings of the 4th International Conference on Bridge Maintenance, Safety and Management 3545-3553.

Cimellaro GP, Reinhorn AM and Bruneau M (2010) Framework for analytical quantification of disaster resilience. Engineering Structures 32(11):3639–3649.

Das R, Pandey AD, Soumya S, Mahesh MJ, Saini P and Anvesh S (2016a) Progressive Collapse of a Cable Stayed Bridge. Procedia Engineering 144:132 – 139.

Das R, Pandey AD, Soumya S and Mahesh MJ (2016b) Assessment of disproportionate collapse behavior of cable stayed bridges. Bridge Structures, 12(1-2):41-51.

Domaneschi M (2012) Experimental and numerical study of standard impact tests on poly-propylene pipes with brittle behaviour. Journal of Engineering Manufacture, Proc. IMechE Part B 226(12):2035–2046.

Domaneschi M, Martinelli L and Perotti F (2016) Wind and earthquake protection of cable-supported bridges. Proceedings of the Institution of Civil Engineers - Bridge Engineering 169(BE3):157–171.

Ghosn M and Moses F (1998) Redundancy in highway bridge superstructures. NCHRP Rep. 406, Transportation Research Board, Washington, DC.

GSA (General Services Administration) (2003) Progressive collapse analysis and design guidelines for new federal office buildings and major modernization projects. GSA, Office of Chief Architect, Washington, DC.

Haberland M, Haß S and Starossek U (2012) Robustness assessment of suspension bridges Bridge Maintenance, Safety, Management, Resilience and Sustainability. Proceedings of the Sixth International Conference on Bridge Maintenance, Safety and Management 1617-1624.

Haifan X (1983) Earthquake analysis of cable-stayed bridges under the action of travelling waves. Journal of Tongji University.

Kanno Y and Ben-Haim Y (2011) Redundancy and robustness, or, when is redundancy redundant? Journal of Structural Engineering ASCE 137(9).

Li S, Li H, Liu Y, Lan C, Zhou W and Ou J (2014) SMC structural health monitoring benchmark problem using monitored data from an actual cable-stayed bridge. Structural Control and Health Monitoring 21(2):156-172.

Liu WD, Ghosn M, Moses F and Neuenhoffer A (2000) Redundancy in highway bridge substructures. NCHRP Rep. 458, Transportation Research Board, Washington, DC

Pastor M, Binda M and Harčarik T (2012) Modal assurance criterion. Procedia Engineering 48:543-548

PTI (Post-tensioning Institute) (2012) Recommendations for stay-cable design, testing and installation. Cable-Stayed Bridges Committee, Phoenix, AZ.

Salem HM and Helmy HM (2014), Numerical Investigation of the Collapse of the Minnesota I-35W Bridge. Engineering Structures 59:635-645.

Starossek U (2008) Collapse resistance and robustness of bridges. IABMAS'08: 4th International Conference on Bridge Maintenance, Safety, and Management Seoul, Korea.

Starossek U and Haberland M (2010). Disproportionate Collapse: Terminology and Procedures. Journal of Performance of Constructed Facilities 24(6):519-528.

Shoghijavan M and Starossek U (2018a) Structural robustness of long-span cable-supported bridges segmented by zipper-stoppers to prevent progressive collapse. IABSE Conference, Kuala Lumpur 2018: Engineering the Developing World – Report 593-600.

Shoghijavan M and Starossek U (2018b) Structural Robustness of Long-Span Cable-Supported Bridges in a Cable-Loss Scenario. Journal of Bridge Engineering ASCE, 23(2):04017133.

Shoghijavan M and Starossek U (2018c) An analytical study on the bending moment acting on the girder of a longspan. Engineering structures 167:166-174.

cable-supported bridge suffering from cable failure

UFC (Unified Facilities Criteria) (2013) Design of buildings to resist progressive collapse. UFC 4-023-03, Dept. of Defense,Washington, DC.

Wang X, Zhu B and Cui S (2017) Research on Collapse Process of Cable-Stayed Bridges under Strong Seismic Excitations. Shock and Vibration art. no. 7185281, 18 pages.

Wolff M and Starossek U (2009) Cable loss and progressive collapse in cable-stayed bridges. Bridge Structures 5(1):17-28.

Wolff M and Starossek U (2010) Cable-loss analyses and collapse behavior of cable-stayed bridges Bridge Maintenance, Safety, Management and Life-Cycle Optimization. Proceedings of the 5th International Conference on Bridge Maintenance, Safety and Management 2171-2178.

Zienkiewicz OC, Taylor RL and Zhu JZ (2005) The Finite Element Method: Its Basis and Fundamentals. Butterworth-Heinemann, Elsevier.

Zong ZH, Huang XY, Li YL and Xia ZH (2016) Study of collapse failure and failure control of long span cable-stayed bridges under strong earthquake excitation. Bridge Construction, 46(1): 24-29.

Figure captions

Figure 1. Modelling of structure to AEM.

Figure 2. Spring interaction between elements in the AEM.

Figure 3. Separation phases.

Figure 4. Stress-strain constitutive law of a bilinear material (a). Tension-only case (b).

Figure 5. Yong-he bridge geometry.

Figure 6. Comparison between FEM and AEM models in terms of mode shapes.

Figure 7. Deformed shape: FEM model and AEM.

Figure 8. Robustness curve.

Figure 9. Load measures needed to calculate redundancy indices.

Figure 10. Absolute value of the acceleration input.

Figure 11. (a) Input accelerogram computed by Haifan (1983). (b) Disproportionate collapse from AEM simulations.

Figure 12. Analysed cables.

Figure 13. Normal stress in cable C6 and C7.

Figure 14. Variation of robustness with respect to time.

Figure 15. (a) New cable configuration and (b) the corresponding AEM model of the bridge.

Figure 16. Axial stresses in the longest cables for the new configuration of the bridge.

Figure 17. Robustness variation with respect to time for the new configuration of the bridge.